Dalton Transactions

ROYAL SOCIETY OF CHEMISTRY

PAPER

View Article Online
View Journal | View Issue

Cite this: *Dalton Trans.*, 2023, **52**, 452

Dual mode antibacterial surfaces based on Prussian blue and silver nanoparticles†

Lavinia Doveri, [a] Angelo Taglietti, [a] Pietro Grisoli,[b] Piersandro Pallavicini [a] and Giacomo Dacarro *[a]

Received 20th September 2022,
Accepted 6th December 2022

DOI: 10.1039/d2dt03058f

rsc.li/dalton

Prussian Blue (PB) is an inexpensive, biocompatible, photothermally active material. In this paper, self-assembled monolayers of PB nanoparticles were grafted on a glass surface, protected with a thin layer of silica and decorated with spherical silver nanoparticles. This combination of a photothermally active nanomaterial, PB, and an intrinsically antibacterial one, silver, leads to a versatile coating that can be used for medical devices and implants. The intrinsic antibacterial action of nanosilver, always active over time, can be enhanced on demand by switching on the photothermal effect of PB using near infrared (NIR) radiation, which has a good penetration depth through tissues and low side effects. Glass surfaces functionalized by this layer-by-layer approach have been characterized for their morphology and composition, and their intrinsic and photothermal antibacterial effect was studied against Gram+ and Gram− planktonic bacteria.

Introduction

Prussian Blue (PB) is an iron containing coordination polymer, known since the 18th century. Accidentally discovered by the German (Prussian, at the times) colour maker Heinrich Diesbach,[1] it has been used for centuries as a blue pigment[2] and, more recently, for its electrochemical, electrochromic, magnetic and electrocatalytic properties.[3] In the last few years, there has been increasing interest for the potential biomedical applications of PB in the fields of imaging and therapy,[4] thanks also to the FDA approval of PB as an antidote for Tl^+ and Cs^+ poisoning. PB is formed by Fe^{3+} cations and hexacyanoferrate(II) complex anions, $[Fe(CN)_6]^{2+}$, the latter being a complex with d^6 Fe^{2+} cations in a low spin state. In PB the Fe^{2+} cations are coordinated by the carbon atom of the cyanide (CN^-) ligand, while Fe^{3+} cations are octahedrally coordinated by 6 nitrogen atoms.

PB shows an intense absorption band in the visible region, centered at 700 nm, due to an intervalence charge transfer of the Fe^{II}/Fe^{III} couple.[5] The absorption band extends in the so-called biological window (750–900 nm) and undergoes thermal relaxation, leading to photothermal heating. This makes PB an ideal candidate for photothermal therapy, showing a photothermal effect comparable to that of metal nanoparticles.[6] To date, the vast majority of the papers treating the photothermal effect of Prussian blue nanoparticles (PBNPs) are devoted to cancer treatment,[7–10] but we recently showed that the same effect can be exploited to exert an antibacterial effect.[11,12] Our study was based on our previous knowledge of the functionalization of surfaces with metal nanoparticles for the preparation of antibacterial and antibiofilm materials.[13–15] In the last few years, some other papers appeared in the literature reporting the antibacterial effect of PBNP and its analogs.[16–18] In the latter case (*i.e.* the PB analogs, coordination polymers where Fe^{II} or Fe^{III} has been replaced fully or partially by another cation) PB loses or changes its typical absorption band, and the effect relies on different mechanisms than the photothermal effect: *e.g.* the release or uptake of cations.[19] Plain PB, on the other hand, has shown good antibacterial performances based on the photothermal ablation of bacteria.[20,21]

In this work we tried to enhance the antibacterial effect of functionalized surfaces, combining a photothermal agent, PBNPs, with a material with intrinsic antibacterial properties: silver nanoparticles (AgNPs). Nanosized silver is a well-known antibacterial agent, and we already tested its efficiency when anchored on Self-Assembled Monolayers (SAMs) on glass surfaces.[13,15,22] Silver also proved to be effective in combination with a photothermally active nanomaterial, *i.e.* gold nanostars.[14] The use of PB could provide a safe and inexpensive alternative to gold nanomaterials, exploiting its ease of synthesis and its biocompatibility.

Some papers report the use of PB in combination with silver, but using different approaches: the examples already present in the literature use PB analogs[19,23] or silver nanoparticles embedded in a PB analog shell. Only one of them

[a]*University of Pavia – Department of Chemistry and Center for Health Technologies; Via Taramelli 12, I-27100 Pavia, Italy. E-mail: giacomo.dacarro@unipv.it*
[b]*University of Pavia – Department of Drug Science; Via Taramelli 12, I-27100 Pavia, Italy*

† Electronic supplementary information (ESI) available. See DOI: https://doi.org/10.1039/d2dt03058f

exploits a dual mode antibactieral effect, but uses a photothermal effect in the visible region, which is hardly exploitable in *in vivo* environments.

In this research work, we thus tried to improve the effect of PBNP functionalized surfaces by adding an overlayer of AgNPs, using the layer-by-layer approach. We believe that this approach can open a new, modular functionalization strategy, easily transferrable to several materials. This could lead to the preparation of novel medical devices and implants capable of preventing the spread of bacterial infections in patients and in nosocomial environments.

A SAM of PBNPs was prepared to anchor PB on an organic polyaminic monolayer,[12] exploiting the electrostatic interaction between negatively charged citrate-coated PBNPs and the positively charged protonated amines. This SAM was then coated with a protective layer of SiO_2, in order to protect it and prevent the interaction between PBNPs and silver. The SiO_2 layer was then further functionalized using the same approach: a grafting layer of silane functionalized polyethyleneimine was used to anchor a layer of AgNPs.

Experimental

Materials

Iron(III) chloride hexahydrate, potassium hexacyanoferrate, citric acid, hydrochloric acid, nitric acid, sulfuric acid, silver nitrate, sodium borohydride, and tetraethyl orthosilicate (TEOS) were purchased from Sigma Aldrich. Trimethoxysilylpropyl(polyethylenimine) (50% in isopropanol) was purchased from Gelest Inc. Reagents and used as received. Solvents were purchased from Sigma-Aldrich and used as supplied. Microscopy cover glass slides (2.2 × 2.6 cm) were purchased from Delchimica. Water was deionized and then distilled. Glassware was carefully cleaned with *aqua regia*, then washed three times with bidistilled water in a sonic bath and oven dried.

Methods and instrumentation

UV-Vis-NIR spectroscopy. A Varian Cary 50 UV-Vis spectrophotometer, Agilent, USA, was used. The wavelength scan range was 300–1100 nm. The samples were placed in a special holder enabling the transmission measurement of the same spot on the slide during all experimental stages.

Contact angle measurement. A KSV CAM200, KSV Instruments, Finland, was used. The static contact angle was measured using water by the sessile drop method.

Scanning electron microscopy (SEM). A Tescan Mira XMU, Tescan USA Inc., USA, was used. Glass slides were mounted on Al stubs and were made electrically conductive by coating them in a vacuum with Pt (thickness 2.5 nm).

Determination of Fe and Ag by ICP-OES. An ICP-OES OPTIMA 3000, PerkinElmer, USA, was used. The total Fe and Ag content on functionalized glass slides was determined by dipping the glass slides in diluted aqua regia (4 : 25 with water) in a beaker and shaking overnight on a Heidolph Promax 1020 reciprocating shaker. After the removal of the glass sample, the resulting solution was sent to ICP-OES measurement without further modifications.

Fe and Ag release experiments were carried out by dipping a glass slide in 3 mL of bidistilled water in a 50 mL beaker for the chosen time (5 h or 24 h). After the chosen release time, the glass was removed and ultrapure HNO_3 was added to the solution up to 4% concentration. Fe and Ag contents were determined by inductively coupled plasma optical emission spectroscopy.

Photo-thermal effect upon near-infrared (NIR) irradiation. PB monolayers were irradiated with NIR light at 808 nm with a multimode AlGaAs laser diode (L808P200, Thorlabs GmbH Dachau/Munich, Germany). The irradiation power used was 200 mW, corresponding to 0.26 Wcm^{-2} irradiance on the sample. The increase in temperature was monitored using an FLIR E40 thermocamera and FLIR Tools+ software (FLIR Systems, Wilsonville, OR, USA).

Studies on planktonic bacteria – determination of the microbicidal effect (ME)

The antibacterial activity of the glasses was investigated against *Staphylococcus aureus* ATCC 6538 (Gram+) and *Escherichia coli* ATCC 10356 (Gram−). The microorganisms were grown overnight in Tryptone Soya Broth (Oxoid; Basingstoke, Hampshire, England) at 37 °C. The washed cells were re-suspended in Dulbecco's PBS 10% and optical density (OD) was adjusted to 0.2 at 600 nm wavelength corresponding approximately to 1×10^8 Colony Forming Units (CFU mL^{-1}). Bacterial suspensions (10 μL) were deposited on a standard microscope slide (76 × 26 mm); subsequently the microbial suspensions were covered with a functionalized glass (22 × 26 mm), forming a thin film between the slides that facilitated direct contact of the microorganisms with the active NP surface. The two assembled glasses were introduced in a Falcon test-tube (50 mL) containing 1 mL of PBS to maintain a damp environment. For each bacterial strain two equivalent modified glasses were prepared; the slides were maintained in contact with liquid films containing bacteria at room temperature for 5 and 24 h, respectively; for each time of contact an unmodified glass slide was processed in parallel as a control sample. After different times of contact, 9 mL of PBS were introduced in each Falcon test-tube under gentle shaking to detach the assembled glass slides. Bacterial suspensions were then grown in Tryptone Soya Agar (Oxoid; Basingstoke, Hampshire, England) to count viable cells. The decimal-log reduction rate, *i.e.* microbicidal effect (ME), was calculated using the formula:

$$ME = \log NC - \log NE$$

where NC is the number of CFU mL^{-1} developed on the unmodified control glasses, and NE is the number of CFU mL^{-1} counted after exposure to modified glasses. The results expressed as ME represent the average of six equivalent determinations.

Photothermal microbicidal effect under NIR irradiation (PME)

The antibacterial activity of NIR irradiation on the glasses was investigated against *S. aureus* ATCC 6538 (Gram+) and *E. coli* ATCC 10356 (Gram−). The microorganisms were grown overnight in Tryptone Soya Broth (Oxoid; Basingstoke, Hampshire, England) at 37 °C. The washed cells were re-suspended in Dulbecco's PBS 10% and optical density (OD) was adjusted to 0.2, at 600 nm wavelength corresponding approximately to 1×10^8 Colony Forming Units (CFU mL^{-1}). Bacterial suspensions (10 μL) were deposited in little wells (20 × 20 mm); subsequently glass slides (22 × 26 mm) were cut into four parts (10 × 10 mm each) and one of these parts was laid down upon bacterial suspensions, forming a thin film between the slides that facilitates direct contact of microorganisms with the active NP surface. Subsequently, the slides were irradiated with continuous laser sources tuned on 808 nm for 30 minutes using an irradiance of 0.26 W cm^{-2} and a beam waist of 1.0 cm (multimode AlGaAs laser diode, L808P200, Thorlabs GmbH, power of radiation 200 mW). After irradiation the inoculum was re-suspended in 1 mL of Dulbecco's PBS 10%; these bacterial suspensions were serially diluted in PBS and were then grown in Tryptone Soya Agar (Oxoid; Basingstoke, Hampshire, England) to count viable cells. The decimal-log reduction rate, microbicidal effect (T-ME), was calculated using the formula: PME = log NCM − log NT (NCM is the number of CFU mL^{-1} developed on the modified but not irradiated control glasses; NT is the number of CFU mL^{-1} counted after exposure to modified and irradiated glasses).

Synthesis of Prussian blue nanoparticles (PBNPs)

PBNPs were synthesized by modifying a previously reported procedure.[12] The concentration of the iron salts was increased from 1 mM (as in the published paper) to 10 mM. In brief, 0.2 mmol $FeCl_3 \cdot 6H_2O$ and 0.5 mmol citric acid were dissolved in 20 mL of water. The solution was kept under stirring at 60 °C. A second solution was prepared with 0.2 mmol $K_4[Fe(CN)_6]$ and 0.5 mmol citric acid in 20 mL of water, heated at 60 °C and added to the Fe(III) solution. The resulting deep blue solution was kept under stirring for 5 min at 60 °C and then at room temperature for 30 min. The solution was centrifuged for 25 min at 13 000 rpm in 10 mL test tubes for purification. The PBNPs pellet was resuspended in the original volume of bi-distilled water.

Synthesis of silver nanoparticles (AgNPs)

AgNPs were synthesized according to a published procedure,[13] without modifications. To 100 mL of ice cooled water the following ice-cooled solutions were added in sequence under vigorous stirring: 1 mL of 1% (w/v) $AgNO_3$ solution, after one minute 1 ml of 1% (w/v) sodium citrate and, after 1 more minute, 0.50 mL of a solution of 0.075% w in $NaBH_4$ and 1% w in sodium citrate.

Preparation of PEI-silane self-assembled monolayers

Firstly, glass substrates were cleaned with fresh *piranha solution* (3 : 1 v/v $H_2SO_4 : H_2O_2$ (30%)) for 30 minutes. (*Caution! Piranha solution is a strong oxidizing agent and should be handled with care.*) The glass slides were washed three times with bi-distilled water in a sonic bath and then dried in an oven at 140 °C. **Glass-PEI** glasses were prepared following a published procedure.[22] Briefly: clean glasses were immersed in a 4% (v/v) solution of PEI-silane in ethanol at room temperature for 6 minutes. Then the slides were washed two times with ethanol and one time with bi-distilled water in a sonic bath and blow-dried with a nitrogen stream. In a typical preparation, 8 glass slides were prepared at the same time, *i.e.* reacting in the same silane solution inside an 8-place holder (a microscope glass slide staining jar).

Grafting of PBNPs on PEI SAMs (Glass-PB)

Glass-PB was prepared according to a published procedure.[12] Shortly **Glass-PEI** glasses were dipped overnight in a PBNP colloid (previously centrifuged and resuspended in the original volume of bi-distilled water). Typically, 8 glass slides were prepared with the same PBNP batch in a microscope glass slide staining jar. After that, the staining jar was filled with bi-distilled water and the samples were sonicated three minutes. Finally the samples were blow dried with nitrogen before use.

SiO_2 coating on Glass-PB (Glass-SiO_2)

Glass-PB was immersed in a solution of 0.3% (v/v) of tetraethyl orthosilicate (TEOS) in ethanol. For a typical 8 glass preparation in a microscope jar, 40 mL of ethanol, 120 μL of TEOS and 403 μL of ammonia were added. After two hours at 40 °C the glasses were washed 2 times for three minutes with fresh ethanol in a sonic bath and then blow dried with nitrogen.

PEI-silane SAMs on Glass-SiO_2

The procedure is already described in the previous paragraph "Preparation of PEI-silane self-assembled monolayers". Briefly, **Glass-SiO_2** glasses were immersed in a 4% (v/v) solution of PEI-silane in ethanol at room temperature for 6 minutes. Then the slides were washed two times with ethanol and one time with bi-distilled water in a sonic bath and blow-dried with nitrogen.

Grafting of AgNPs (Glass-PB/Ag)

Glass-PB/Ag was obtained by dipping **Glass-SiO_2** functionalized with PEI silane in an AgNP colloidal solution (prepared the day before) for 15 minutes. This procedure was adapted from a well-established procedure for the preparation of AgNPs monolayers on an amino-terminated SAM.[22] After that time the glasses were washed 2 times with fresh bi-distilled water and blow-dried with nitrogen.

Results and discussion

Choice of the functionalization strategy

In preliminary screening, we tested different approaches to achieve a multilayer (or a mixed monolayer containing both silver and PB nanoparticles). The easier approach would be

immersing a PEI-silane slide in a AgNP colloid and later in a PBNP colloid, or *vice versa*. Both of these strategies led to the complete degradation of the first layer of particles (see S2 for experimental details and spectroscopic data), probably due to the formation of silver hexacyanoferrate.[24] This simple approach is thus not viable, and the first grafted layer of inorganic nanoparticles needs to be appropriately protected before the second nanomaterial is anchored on the surface.

The best strategy to combine two different materials on the same substrate, PBNPs and AgNPs, avoiding their reaction was therefore the layer-by-layer approach, using a thin layer of silica to physically isolate PB from silver and prevent any side reactions. The use of silica allows us to maintain the transparency needed for the photothermal effect. We adopted an approach that our group used previously for the formation and protection of a monolayer of gold nanostars and further grafting of a AgNP monolayer.[14] The synthetic pathway is sketched in Fig. 1.

Characterization of single steps

Each step in the LbL process was characterized by means of UV-Vis spectroscopy and contact angle measurement. The two techniques are non-destructive and easily available and can be used for a routine check of functionalization. The steps which can lead to a relevant change in the morphology of the substrates (*i.e.* **Glass-PB**, **Glass-SiO$_2$** and **Glass-PB/Ag** layer) were also analyzed by SEM imaging, in order to track any changes in the shape and distribution of the grafted particles.

Contact angle measurement. Contact angle measurement and UV-Vis spectroscopy are non-destructive, inexpensive techniques that can be applied as a routine control on all the prepared samples. All the functionalization steps were characterized through static water contact angle measurements. The results, expressed as average values and standard deviations, are reported in Table 1.

The first layer of nanoparticles is formed by PB nanocubes (see S1 for TEM imaging of the colloid) and its contact angle value, 6°, indicates high hydrophilicity. The value is also significantly different from the contact angle of the underlying monolayer of PEI-silane (not reported in the table) which is typically around 41°.[22] Deposition of a silica overlayer leads also to a very low CA, 7°, diagnostic of a highly hydrophilic surface and perfectly compatible with what we reported before for a gold nanostar monolayer coated with SiO_2.[14] The formation of a PEI-silane monolayer on top of SiO_2 leads to a CA of 22°, lower than the PEI SAM on glass, but still significantly different from the CA of the underlying layer. Moreover, it has to be stressed that the CA of polyamines can be strongly dependent on the morphology and protonation.[25,26] The difference between this layer and the first PEI SAM is thus not surprising. The deposition of AgNPs does not significantly change the CA value of the underlying amino-terminated SAM, as we previously reported for a similar material (*i.e.* AgNP layer on the APTES SAM).[14]

Table 1 Static water contact angle values for each step of the LbL process

Sample	CA (°)
Glass-PB	6(2)
Glass-SiO_2	7(2)
Glass-SiO_2/PEI	22(1)
Glass-PB/Ag	23(3)

Each value is the average of the measurements taken on three samples (four measurements for each sample). Standard deviation in parentheses.

CA measurement allows us to follow the LbL process with a quick, non-destructive technique. Some of the steps, however, do not show significant differences in the CA values and require further characterization with other techniques, as shown in the following paragraphs.

UV-Vis spectroscopy. Functionalized glass slides were also characterized by UV-Vis spectroscopy, in order to identify the presence of PBNPs and AgNPs, both bearing a diagnostic and intense visible absorption.

The first layer with a spectrum significantly different from bare glass is **Glass-PB:** the spectrum shows a typical absorption band centered at 700 nm, diagnostic of the presence of Prussian blue nanocrystals. Coating the PBNP layer with TEOS (*i.e.* a silica layer) induces a blue shift in the maximum absorp-

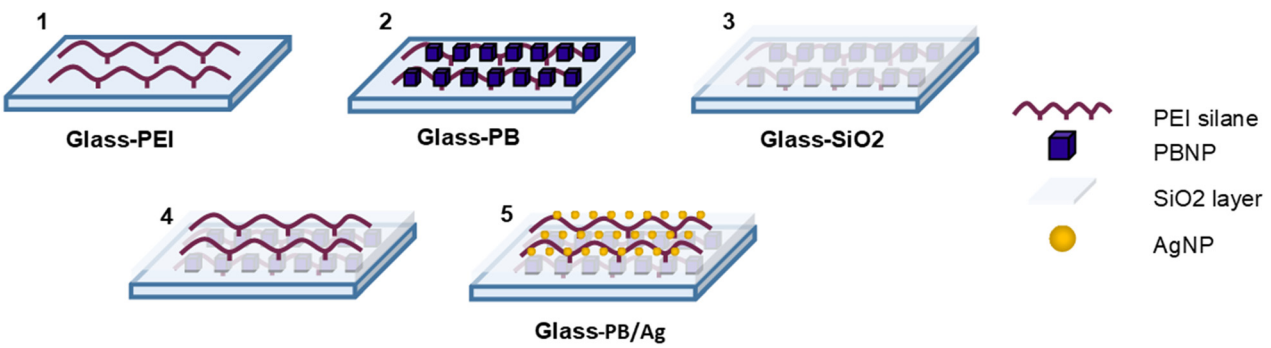

Fig. 1 The scheme depicts the approach adopted for the layer-by-layer functionalization of a glass slide. (1) Deposition of a polyaminic self-assembled monolayer on a glass slide, (2) grafting of PBNPs, (3) protection of the PBNP layer with a thin layer of silica, (4) second grafting layer of polyamino silane and (5) grafting of AgNPs.

tion wavelength and a decrease in the absorbance. It has been previously reported[27] that PB undergoes a slight shift in its maximum absorption wavelength when PBNPs are suspended in different solvents. Moreover, it has been reported that SiO_2 coating on mesoporous PBNPs induces a significant blue-shift and a decrease in absorbance.[28] The same effect can be at the origin of the blue-shift and intensity decrease we observed upon changing from **Glass-PB** to **Glass-SiO$_2$** samples.

After the deposition of PEI-silane and successive AgNP grafting (**Glass-PB/Ag** sample, the green line in Fig. 2) two distinct bands appear in the UV-Vis spectrum: PBNP band is shifted back to the original maximum absorption wavelength, 704 ± 3 nm, while the diagnostic LSPR band of silver nanoparticles is present at 393 ± 5 nm (all the values are calculated with the average of 8 samples). The last functionalization step seems to lead to a decrease in the PBNP band intensity. A quantitative evaluation, however, is difficult due to the incomplete resolution of the bands and to the high FWHM. Better quantification of the PBNPs can be achieved by means of ICP-OES analysis, described in the next paragraph.

Glass-PB/Ag samples are homogeneous all over the surface (*i.e.* spectra recorded in different spots of the sample are similar) and are stable in air for months.

ICP-OES elemental analysis. Total quantities of Fe and Ag grafted in the successive functionalization steps were determined in solution through ICP-OES analysis, after complete oxidation of the metals (see Experimental for details). The total metal quantity was then related to the sample surface, obtaining a surface concentration of metal ions (expressed as μg cm^{-2}), as shown in Table 2.

The iron concentration on the PBNP monolayer is coherent with what we previously published for a SAM made using the same procedure.[12] Deposition of a SiO_2 layer does not induce a significant variation in the Fe concentration. This confirms that the differences in the UV-Vis spectra described in the previous paragraph must be due only to the change in the optical properties of the material, and not to a loss of Fe ions or PBNPs.

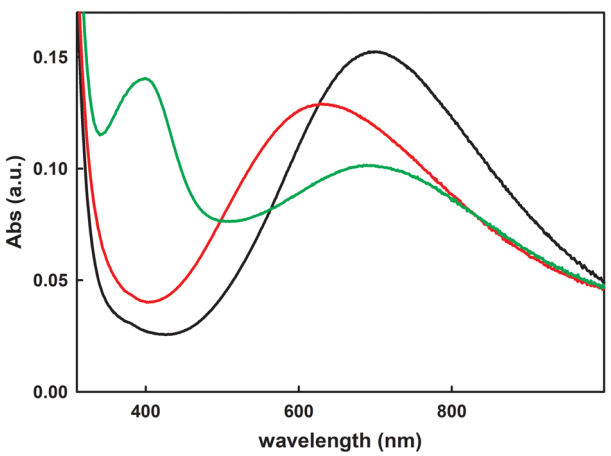

Fig. 2 Representative UV-Vis spectra for each functionalization step. Black line: **Glass-PB**, red line: **Glass-SiO$_2$**, and green line **Glass-PB/Ag**.

Table 2 Total Fe and Ag quantities determined by ICP-OES

Sample	Fe (μg cm^{-2})	Ag (μg cm^{-2})
Glass-PB	0.40(3)	
Glass-SiO_2	0.37(4)	
Glass-PB/Ag	0.23(2)	0.25 ± 0.05

Each value is the average of the measurements taken on three samples. Standard deviation on the last figure is in parentheses.

In **Glass-PB/Ag** the Ag concentration is lower than what we reported previously for a AgNP monolayer.[13,22] The value of surface concentration found in our experiments is about 65% of what we found for a simple SAM of AgNPs on a thiol-terminated silane layer.

Besides evaluating the total quantity of iron and silver loaded on the glass samples, we also wanted to evaluate the release of metal ions in water from Glass-PB/Ag samples. This was done with release experiments in 3 mL of bidistilled water at 5 and 24 hours (as described in the Materials and methods section). The chosen release times are the same used for antibacterial activity tests described in paragraph 3.3.1. Fe ions release is comparable with what we previously found for a Glass-PB type surface:[12] ≈15% of the total Fe is released at 5 and 24 hours, with a Fe concentration in the experiment volume of ≈3 × 10^{-6}, which can be considered completely harmless in a biological environment. Moreover, UV-Vis spectroscopy on the release solution did not show any absorption peaks: this allows us to rule out the detachment of nanoparticles, ascribing the detected Fe in water only to the release of ions.

The measured release of Ag ions was 0.13 μg cm^{-2} at 5 hours and 0.18 μg cm^{-2} at 24 hours. These values are higher than those found for monolayers of silver nanoparticles on silane SAMs (*i.e.* thiol[13] or amino modified surfaces[15,22]) but are comparable to what we found for a monolayer of AgNPs grafted on a thin layer of silica in a multi-layered material.[14] This data thus confirm that a higher release of silver ions is obtained when silver nanoparticles are grafted on a less regular surface like a silica layer grown over a nanostructured surface. Silver release, in all the mentioned studies, is higher in the first few hours and reaches a steady state for longer periods. UV-Vis measurements on the released solutions confirmed that, as we reported for PBNPs, the LSPR band of AgNPs is totally absent in the measured solutions, confirming that silver is released only in ionic form, and not as metal nanoparticles. This helps to rule out potential toxicity related to the release of nanostructured metallic silver in the biological environment. Under the conditions of our experiment (*i.e.* a 11.44 cm^2 sample in 3 mL of bidistilled water), the released silver ion concentration was 0.95 μg mL^{-1}. The level of released silver ions is well below the concentrations that can cause any toxicity-related issues. Typically a concentration of tens-hundred of milligrams per kg bodyweight is required to exert any negative effects.[29]

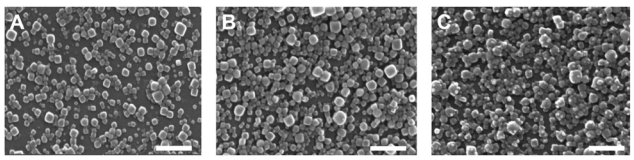

Fig. 3 SEM micrographs of the different functionalization steps. Each micrograph has 250k× magnification. White scale bar measures 250 nm: (A) **Glass-PB**; (B) **Glass-SiO$_2$** and (C) **Glass-PB/Ag**.

SEM imaging. Glass-PB, **Glass-SiO$_2$** and **Glass-PB/Ag** samples were characterized thanks to SEM microscopy imaging, in order to confirm the morphology of the nanoparticles after their anchoring on glass slides. Fig. 3 shows a representative micrograph for each of the above-mentioned layers.

Fig. 3A shows the typical shape and size of PBNP nanocubes, compatible with what we found with TEM measurements on the PB colloid (see ESI†). The deposition of a SiO_2 layer (Fig. 3B) does not show a significant modification in the nanoparticle morphology. Measuring 150 particles on each sample (*i.e.* **Glass-PB** and **Glass-SiO$_2$**) the average sizes are 31 ± 12 nm and 31 ± 10 nm, respectively. Both average size measurements are not significantly different from what we found on TEM imaging (29 ± 8 nm). It is thus reasonable to estimate that the thickness of the SiO_2 layer is a few nanometers, as expected from the chosen experimental conditions.[14] The actual presence of SiO_2 is nevertheless confirmed by a change in the optical properties reported in paragraph 3.2.2 and by the fact that the deposition of AgNPs in the absence of a SiO_2 layer is not possible (as shown in S2).

Fig. 3C clearly shows the presence of AgNPs on top of the PBNPs. This further confirms the presence of silver (which was already detected and quantified by means of ICP-OES, as described in the previous paragraph) and further confirms the fact that silver is present as nanoparticles, as expected from the presence of an LSPR band in the UV-Vis spectra.

Photothermal effect. We recently demonstrated that PBNP monolayers show a remarkable photothermal effect which can be exploited for antibacterial action.[12] The effect is retained in all the LbL functionalization steps of the hybrid material presented in this paper, *i.e.* **Glass-PB**, **Glass-SiO$_2$** and **Glass-PB/Ag**. The results are shown in Table 3 and a representative thermogram for each step is shown in Fig. 3.

Glass-PB samples showed a thermal increase of 13.3 K after 60 seconds of irradiation, a value comparable with what we previously reported for the same material. **Glass-SiO$_2$** and **Glass-PB/Ag** show lower values of ΔT, but this is not surprising as these samples have a lower absorbance at the wavelength of irradiation.

To further confirm this dependence, which is always verified for the photothermal effect of nanoparticles, we plotted the ΔT values of the three different functionalization steps as a function of the absorbance at 808 nm. As shown in panel A of Fig. 4 hyperthermia is linearly dependent on the absorbance at the wavelength of irradiation. **Glass-SiO$_2$** and **Glass-PB/Ag** have different maximum absorbances, but the spectra at 808 nm are almost superimposed. The ΔT values are thus completely similar.

It must be remarked that even a small increase in temperature can be crucial for exerting an efficient bactericidal effect. A 9 K variation (as reported for **Glass-PB/Ag** samples) can indeed increase the local temperature from physiological 37° to 46° degrees, enough to activate the irreversible effects of hyperthermia in the cells.

Table 3 Photothermal effect (as ΔT(K) after 60 s of irradiation at 0.255 W cm^{-2})

Sample	ΔT (K)
Glass-PB	13.3(9)
Glass-SiO$_2$	9.2(5)
Glass-PB/Ag	8.9(5)

Each value is the average of the measurements taken on three samples. Standard deviation in parentheses.

Antibacterial effect

Prussian blue has no intrinsic antibacterial effects, since this coordination polymer is nontoxic and perfectly biocompatible. Moreover, nanoparticles on a SAM are firmly anchored and their release in solution is negligible. We thus previously demonstrated that a PBNP SAM anchored on PEI-silane (*i.e.* a **Glass-PB** sample) has no antibacterial effect against Gram+ and Gram− bacteria. A limited effect can however be obtained by exploiting the photothermal effect of these surfaces.[12]

Intrinsic antibacterial effect. Glass-PB/Ag substrates bear a top layer of AgNPs which are intrinsically antibacterial. We thus tested their activity against representative Gram+ and Gram− bacteria: *S. aureus* and *E. coli*, respectively. Tests were performed against planktonic bacterial cells at different

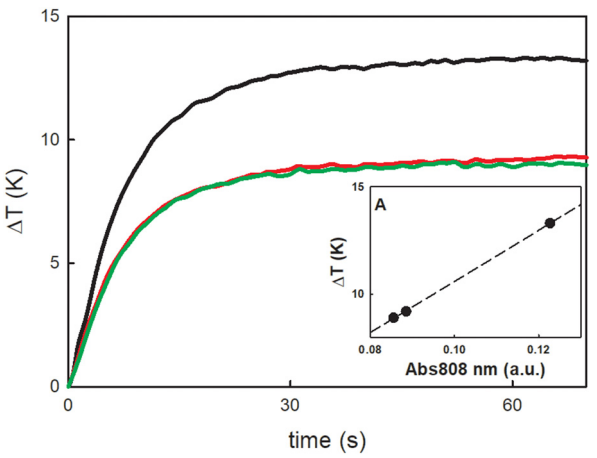

Fig. 4 Photothermal effect. Black: **Glass-PB**, red: **Glass-SiO$_2$**, and green: **Glass-PB/Ag**, irradiated at λ = 808 nm, I = 0.255 W cm^{-2}. Fig. 3A (inset) shows the ΔT *vs.* absorbance relationship at 808 nm for the three examined samples. The effect on glass slides without a PB coating is negligible and not reported in the figure.

contact times: 5 hours and 24 hours. The microbicidal effect (ME) was expressed as logarithmic units using eqn (1):

$$ME = \log N_C - \log N_E. \quad (1)$$

In eqn (1), N_C represents the CFU mL^{-1} (colony forming units) number counted on a reference sample (*i.e.* a clean, non-functionalized glass slide) while N_E is the CFU mL^{-1} number counted on functionalized glass.

The results shown in Table 4 show a significant effect against both strains.

The results are compatible with what we reported in previous studies on silver nanoparticles anchored on different monolayers.[13,22] The intrinsic effect at 24 h of **Glass-PB/Ag** is also comparable with a material combining photothermally active gold nanostars and silver nanoparticles, studied in a previous work of our research group.[14] In comparison with gold nanostars/silver nanoparticle hybrid materials, **Glass-PB/Ag** has a higher intrinsic effect for the 5 h incubation time. Silver nanoparticles always show a greater effect against Gram− bacteria, leading to the complete elimination of the viable cells (*i.e.* logarithmic effects greater than 5–6 units). The effect against Gram+ bacteria is always lower on this kind of surface, probably due to the presence of a thicker peptidoglycan cell wall. It has to be stressed, however, that a 1.4–1.6 logarithmic unit effect against *S. aureus* means that more than 95% of the bacterial cells are killed at the given times.

Photothermal antibacterial effect. In order to evaluate the switchable photothermal antibacterial effect a different experiment was performed: functionalized glasses were put in contact with a planktonic suspension of bacteria (similarly to the intrinsic effect test) and irradiated for 30 minutes with a low irradiance (*i.e.* 0.255 W cm^{-2}).

The results shown in Table 5, expressed as logarithmic units, show significant effects against Gram+ and Gram− bacteria at shorter times, when irradiation is used to improve the antibacterial effect. The results are compared with what we obtained from a PBNP monolayer anchored on a PEI SAM (*i.e.* the **Glass-PB** stage of the samples presented in this paper). The small photothermal microbicidal effect exerted by PBNPs alone is significantly increased when the intrinsic effect of silver is added. Considering the effect on Gram− bacteria (*E. coli* in our tests) an intrinsic effect is present also at the shorter incubation times used in these tests, in 30 minutes the effect is 1.7 logarithmic units. This effect is strongly increased, reaching 4.7 units. The effect is higher than the 3.3 units measured in the presence of the sole PBNP monolayer. For **Glass-PB/Ag** the effect is a sum of the intrinsic effect of silver and of the photothermal effect of Prussian blue, leading to almost complete elimination of viable bacterial cells in 30 minutes.

Regarding the effect against Gram+ bacteria (*S. aureus*) in the absence of irradiation, the effect is low and not clearly discernible from the value reported without AgNPs. A significant and much higher effect, however, is measured in the presence of irradiation at 808 nm: 1.5 units of PME are measured for **Glass-PB/Ag** samples, while the effect is null for the sole PBNP monolayer. The presence of silver is thus increasing considerably the effect, in combination with the photothermal action of PBNPs. An effect of 1.5 logarithmic units corresponds to the elimination of ≈97% of the viable bacterial cells. Under irradiation this effect is obtained in 30 minutes, a much shorter time with respect to the 5 hours needed to obtain a comparable effect in the absence of irradiation, *i.e.* relying on the intrinsic effect of silver only.

Interaction mechanism. A complete exploration of the interaction mechanism of these new materials with bacteria was out of the scope of the paper, but some consideration can however be made based on literature data and theoretical knowledge. The intrinsic effect of silver nanoparticles is mainly based on the release of silver ions. As we previously demonstrated in a previous work, a monolayer of AgNPs exposed to a water environment undergoes progressive oxidation to silver oxide, with a constant release of silver ions in time.[30]

Furthermore, silver nanoparticles typically show a broad antibacterial spectrum, being active against at least 12 species of bacteria including several resistant strains.[31] Nanosilver has also antifungal, antiviral, and antiprotozoal activities[32] and can control vector-borne infections.[33]

The photothermal effect, on the other hand, relies simply on local hyperthermia that can disrupt malignant cells and bacteria by heating. As we discussed in the dedicated paragraph in this paper, even a small temperature increase (*i.e.* around 10 °C in our case) can lead to a significant decrease in the bacterial cell viability. Crucial parameters for the photothermal effect are the time of irradiation, the irradiation wavelength and the power density of the laser. In our study, we irradiated the samples at

Table 4 Microbicidal effect (ME) of **Glass-PB/Ag** samples against Gram+ *S. aureus* and Gram− *E. coli*, at 5 and 24 hours of incubation time

	ME	
Bacterial strain	5 h	24 h
E. coli	>7	>7
S. aureus	1.4(8)	1.6(8)

Each value is the average of 3 measurement repetitions. Standard deviation in parentheses.

Table 5 Photothermal microbicidal effect (PME) against Gram+ *S. aureus* and Gram− *E. coli*, with and without 30′ irradiation at 808 nm and 0.255 W cm^{-2} irradiance

	PME Glass-PB/Ag		PME Glass-PB[12]	
Bacterial strain	NL	L	NL	L
E. coli	1.7(5)	4.7(9)	0.1(1)	3.3(5)
S. aureus	0.6(6)	1.5(3)	0.3(4)	0.1(7)

Each value is the average of 3 measurement repetitions. Standard deviation on the last digit in parentheses. Values for the photothermal microbicidal effect in the absence of AgNPs (*i.e.* of the **Glass-PB** SAM only) are reported in ref. 11. NL = no laser irradiation; L = laser irradiation.

808 nm for 30 minutes using an irradiance of 0.26 W cm^{-2} and a beam waist of 1.0 cm. It must be stressed that most of the studies on photothermal nanomaterials (metals, polymers or carbon based) use higher irradiances: *e.g.* 1 W cm^{-2}.[34] We chose to work at an irradiance below the ANSI standards for skin irradiation (*i.e.* 0.32 W cm^{-2} at 800 nm),[35] in the perspective of potential *in vivo* use of these materials. The photothermal effect, as already reported in the literature, is a powerful tool that can also overcome the resistance of Gram+ and Gram− bacteria.[34]

Conclusions

In this paper we presented a new material prepared using the layer-by-layer approach. The material combines photothermally active Prussian blue nanoparticles and intrinsically antibacterial silver nanoparticles. Prussian blue is an FDA approved material and is completely biocompatible and its photothermal effect is well known. Silver, on the other hand, has been extensively studied for its potential in antibacterial materials and preparations. Several studies demonstrated that silver-decorated surfaces are non-cytotoxic.[36,37] The photothermally active layer of PB is anchored on a SiO_2 surface exploiting an organic SAM as an anchoring layer. PB is then covered with a thin layer of silica, in order to protect it from undesired reactions with silver and to add mechanical and chemical stability, thus improving its durability. Silver nanoparticles, on the other hand, are grafted on the SiO_2 layer and exposed on the surface in order to be able to exert their effect. Antibacterial activity tests demonstrated that these materials have a good intrinsic effect against Gram− and Gram+ bacteria and, most importantly, this effect can be increased and accelerated in the presence of irradiation at 808 nm. The use of an irradiation wavelength in the near infrared region opens the possibility of using these materials *in vivo*, with trough tissue irradiation. The photothermal effect can be activated with a low-irradiance laser, complying with the standards for *in vivo* use. The surface functionalization strategy presented in this paper can thus be employed for the functionalization of internalized devices, applying the same synthetic procedure on polymeric or inorganic materials commonly used in biomedical devices and implants. This could help in answering the increasing need for new materials capable of preventing the spreading of infections and the formation of biofilms.

Compliance with ethical standards

Experiments did not involve any human or live subjects. All experiments were performed in compliance with relevant laws or guidelines.

Author contributions

Giacomo Dacarro: conceptualization, methodology, investigation, and writing – original draft preparation. Lavinia Doveri: methodology, investigation, writing – review & editing, and validation. Piersandro Pallavicini: funding acquisition, supervision, and conceptualization. Angelo Taglietti: funding acquisition, supervision, and conceptualization. Pietro Grisoli: investigation and methodology.

Conflicts of interest

There are no conflicts to declare.

Acknowledgements

This research was funded by Regione Lombardia, Innovation HUB, CE4WE. The authors thank Dr Lucia Cucca of the Department of Chemistry, University of Paiva, for the ICP-OES measurements.

References

1 M. Ware, *J. Chem. Educ.*, 2008, **85**, 612.
2 F. Grandjean, L. Samain and G. J. Long, *Dalton Trans.*, 2016, **45**, 18018–18044.
3 X. Du, X. Hao, Z. Wang and G. Guan, *J. Mater. Chem. A*, 2016, **4**, 6236–6258.
4 J. Long, Y. Guari, C. Guérin and J. Larionova, *Dalton Trans.*, 2016, **45**, 17581–17587.
5 B. Kong, C. Selomulya, G. Zheng and D. Zhao, *Chem. Soc. Rev.*, 2015, **44**, 7997–8018.
6 G. Fu, W. Liu, S. Feng and X. Yue, *Chem. Commun.*, 2012, **48**, 11567–11569.
7 H. A. Hoffman, L. Chakrabarti, M. F. Dumont, A. D. Sandler and R. Fernandes, *RSC Adv.*, 2014, **4**, 29729.
8 G. Dacarro, A. Taglietti and P. Pallavicini, *Molecules*, 2018, **23**, 1–20.
9 M. Gautam, K. Poudel, C. S. Yong and J. O. Kim, *Int. J. Pharm.*, 2018, **549**, 31–49.
10 P. Wang, R. K. Kankala, B. Chen, Y. Zhang, M. Zhu, X. Li, R. Long, D. Yang, R. Krastev, S. Wang, X. Xiong and Y. Liu, *ACS Appl. Mater. Interfaces*, 2021, **13**, 37563–37577.
11 M. Borzenkov, L. D'Alfonso, A. Polissi, P. Sperandeo, M. Collini, G. Dacarro, A. Taglietti, G. Chirico and P. Pallavicini, *Nanotechnology*, 2019, **30**, 295702.
12 G. Dacarro, P. Grisoli, M. Borzenkov, C. Milanese, E. Fratini, G. Ferraro, A. Taglietti and P. Pallavicini, *Supramol. Chem.*, 2017, **29**, 823–833.
13 P. Pallavicini, A. Taglietti, G. Dacarro, Y. A. Diaz-Fernandez, M. Galli, P. Grisoli, M. Patrini, G. Santucci De Magistris and R. Zanoni, *J. Colloid Interface Sci.*, 2010, **350**, 110–116.
14 P. Pallavicini, B. Bassi, G. Chirico, M. Collini, G. Dacarro, E. Fratini, P. Grisoli, M. Patrini, L. Sironi, A. Taglietti, M. Moritz, I. Sorzabal-Bellido, A. Susarrey-Arce, E. Latter, A. J. Beckett, I. A. Prior, R. Raval and Y. A. Diaz Fernandez, *Sci. Rep.*, 2017, **7**, 1–10.

15 A. Taglietti, C. R. R. Arciola, A. D'Agostino, G. Dacarro, L. Montanaro, D. Campoccia, L. Cucca, M. Vercellino, A. Poggi, P. Pallavicini, L. Visai, P. Pallavicini and L. Visai, *Biomaterials*, 2014, **35**, 1779–1788.
16 J. Li, X. Liu, L. Tan, Z. Cui, X. Yang, Y. Liang, Z. Li, S. Zhu, Y. Zheng, K. W. K. Yeung, X. Wang and S. Wu, *Nat. Commun.*, 2019, **10**, 4490.
17 Z. Wang, B. Yu, H. Alamri, S. Yarabarla, M.-H. Kim and S. D. Huang, *Angew. Chem., Int. Ed.*, 2018, **57**, 2214–2218.
18 D. Li, M. Liu, W. Li, Q. Fu, L. Wang, E. Lai, W. Zhao and K. Zhang, *Pharmaceuticals*, 2022, **15**(7), 769.
19 S. Mukherjee, R. Kotcherlakota, S. Haque, S. Das, S. Nuthi, D. Bhattacharya, K. Madhusudana, S. Chakravarty, R. Sistla and C. R. Patra, *ACS Biomater. Sci. Eng.*, 2020, **6**, 690–704.
20 S. Cai, J. Qian, S. Yang, L. Kuang and D. Hua, *Colloids Surf., B*, 2019, **181**, 31–38.
21 H. Maaoui, R. Jijie, G.-H. Pan, D. Drider, D. Caly, J. Bouckaert, N. Dumitrascu, R. Chtourou, S. Szunerits and R. Boukherroub, *J. Colloid Interface Sci.*, 2016, **480**, 63–68.
22 G. Dacarro, L. Cucca, P. Grisoli, P. Pallavicini, M. Patrini and A. Taglietti, *Dalton Trans.*, 2012, **41**, 2456–2463.
23 S. Sharma, N. Chakraborty, D. Jha, H. K. Gautam and I. Roy, *Mater. Sci. Eng., C*, 2020, **113**, 110982.
24 W. Huang, Y. Liang, Y. Deng, Y. Cai and Y. He, *Microchim. Acta*, 2017, **184**, 2959–2964.
25 M. Khalid, N. Wasio, T. Chase and K. Bandyopadhyay, *Nanoscale Res. Lett.*, 2010, **5**, 61–67.
26 S. Flink, F. C. J. M. Van Veggel and D. N. Reinhoudt, *J. Phys. Org. Chem.*, 2001, **14**, 407–415.
27 T. Uemura and S. Kitagawa, *J. Am. Chem. Soc.*, 2003, **125**, 7814–7815.
28 X. Mei, Y. Han, J. Xi, J. Liu, L. Xu, J. Yuan, S. Wang, X. Li, W. Si and J. Li, *Mater. Lett.*, 2022, **312**, 131697.
29 N. Hadrup, A. K. Sharma and K. Loeschner, *Regul. Toxicol. Pharmacol.*, 2018, **98**, 257–267.
30 P. Pallavicini, A. Taglietti, G. Dacarro, Y. A. Diaz-Fernandez, M. Galli, P. Grisoli, M. Patrini, G. Santucci De Magistris and R. Zanoni, *J. Colloid Interface Sci.*, 2010, **350**, 110–116.
31 H. H. Lara, E. N. Garza-Treviño, L. Ixtepan-Turrent and D. K. Singh, *J. Nanobiotechnol.*, 2011, **9**, 30.
32 M. Rai, A. Yadav and A. Gade, *Biotechnol. Adv.*, 2009, **27**, 76–83.
33 M. Rai, K. Kon, A. Ingle, N. Duran, S. Galdiero and M. Galdiero, *Appl. Microbiol. Biotechnol.*, 2014, **98**, 1951–1961.
34 S. Yougbaré, C. Mutalik, D. I. Krisnawati, H. Kristanto, A. Jazidie, M. Nuh, T.-M. Cheng and T.-R. Kuo, *Nanomaterials*, 2020, **10**(6), 1123.
35 ANSI, *American National Standard for Safe Use of Lasers Outdoors*, Laser Institute of America, 13501 Ingenuity Drive, Suite 128 Orlando, FL 32826, 2015.
36 M. Ai, Z. Du, S. Zhu, H. Geng, X. Zhang, Q. Cai and X. Yang, *Dent. Mater.*, 2017, **33**, 12–22.
37 S. Taheri, A. Cavallaro, S. N. Christo, L. E. Smith, P. Majewski, M. Barton, J. D. Hayball and K. Vasilev, *Biomaterials*, 2014, **35**, 4601–4609.